EES Batteries

ROYAL SOCIETY OF CHEMISTRY

PAPER

View Article Online
View Journal

Cite this: DOI: 10.1039/d5eb00096c

Mitigation of resistance increase in positive electrodes of lithium-ion batteries during floating–cycling by operating voltage control

Tetsuya Omiya, [a] Atsunori Ikezawa, [a] Keita Takahashi,[b] Keiichi Saito,[b] Masao Yonemura, [c] Takashi Saito, [c] Takashi Kamiyama, [c,d,e] Kazuhiro Mori [c] and Hajime Arai *[a,c]

Received 16th May 2025,
Accepted 31st July 2025

DOI: 10.1039/d5eb00096c

rsc.li/EESBatteries

As the use of lithium-ion batteries (LIBs) is widespread, understanding the degradation factors as well as life extension of LIBs is of great importance. While the LIBs are often continuously charged (float-charged) and occasionally discharged, such a mixture of floating and cycling causes severe capacity loss, which is much worse than the sum of mere floating and mere cycling. In this work, durability tests of commercially available 18 650 LIB cells were performed for more than 2 years in the floating–cycling mode, and the effects of charging voltage limitation and depth of discharge restriction on degradation were evaluated. The aged cells were analyzed using voltage profiles, impedance measurements and operando neutron diffraction, which showed that the resistance increase in the positive electrode as the main origin of degradation can be alleviated with the charging voltage limitation rather than the depth of discharge limitation. The post-mortem analysis of an aged positive electrode indicated that the microcracks caused by cycling were covered with resistive films formed by the floating operation, which was mitigated by the charging voltage limitation. These results will give insights into the capacity loss in LIBs and contribute to LIB life extension.

Broader context

A huge number of lithium-ion batteries (LIBs) are produced worldwide for mobile, backup and automobile applications. While LIB-based energy storage systems can generally contribute to the effective use of energy and reduce CO_2 emission from our society, the CO_2 emission associated with LIB production cannot be disregarded, which includes high-temperature calcination for material synthesis and the use of dry rooms (water-free environment) for cell fabrication. Therefore, maximizing the utilization period (lifetime) of LIBs is essential to reduce the life-cycle CO_2 emission of LIBs. This study shows how commercially available LIBs degrade under float-charging with periodic discharging conditions and what operational parameters are essential to alleviate the degradation. The life extension method shown in this study will contribute to reducing the lifetime CO_2 emissions of LIBs.

1 Introduction

Lithium-ion batteries (LIBs) with layered positive and graphite negative electrodes have high energy density and long cycle life, and have been widely applied as power sources for portable devices, electric vehicles and stationary power storage applications.[1–4] Considering the resources and energy used for manufacturing these cells, it is essential to understand the major cell degradation factors and to take measures to prolong their lifetime, especially for long-term power supply applications. As detailed in several reviews,[5–9] the most commonly recognized degradation mode of LIBs is loss of lithium inventory (LLI), where the amount of available lithium originally extracted from the positive electrode is consumed by side reactions at the graphite negative electrode, which shifts the potential windows of both electrodes.[10–15] Charge–discharge cycles at high temperatures and high voltage cause thick negative electrode film formation, leading to high cell impedance and serious degradation.[16–18] Fast and low-temperature charging leads to metallic lithium deposition at the graphite negative electrode, which also causes LLI and occasionally short circuits.[19,20] The other important degradation mode is the loss

[a]Institute of Science Tokyo, 4259, Nagatsuta, Yokohama, Midori-ku, Kanagawa, 226-8501, Japan. E-mail: arai.h.9d0c@m.isct.ac.jp
[b]NTT Anode Energy Corporation, Granparktower, 3-4-1 Shibaura, Minato-ku, Tokyo, 105-0023, Japan
[c]High Energy Accelerator Research Organization, 203-1, Oazashirane, Tokai, Naka, Ibaraki, 319-1195, Japan
[d]Institute of High Energy Physics, Chinese Academy of Sciences, Beijing, 100049, China
[e]Spallation Neutron Source Science Center, Dongguan, 523803, China

of active materials (LAM), which is often associated with high current load and high voltage operation, and is derived from particle cracking and element dissociation at the positive electrode, which decrease the effective mass of the active material.[10,21] Surface rock-salt phase formation is also reported to be detrimental in nickel-rich positive electrode materials.[22,23]

In our previous study, we focused on cell degradation under continuous (float) charging conditions.[24] The background is that the cells in backup applications are connected in parallel with commercial power sources and load, and are continuously float-charged, whereas such continuous charging can lead to resistive film formation, LLI, and transition metal dissolution.[25] The same phenomena can also be applied to many portable devices, such as cellular phones that are connected to commercial power sources at home and in the office and continuously charged. Motivated by this background, we compared the degradation of cells under float charging and those under continuous charging with occasional (or periodic) discharge processes, which could suppress possible degradation by the floating and allow the utilization of the accumulated power for peak-cutting and peak-shifting (using low-demand and low-price power to high-demand and high-price power).[24] In contrast to our expectation, it turned out that the combination of floating and occasional discharging, called the floating–cycling mode, causes serious capacity loss of more than 20% per year, which is much more than the degradation sum of mere floating and mere cycling modes. The main origin of the degradation has been attributed to the resistance increase in the positive electrode (RIPE), which seems to be caused by electrode particle cracking due to cycling and film formation at the cracked electrode surface. While the cells in the previous study were charged at 4.2 V and discharged to 2.5 V to utilize the full cell capacity, either restricting the charging voltage or limiting the depth of discharge could be effective in suppressing the serious RIPE degradation during floating–cycling.

In this study, we focus on the degradation of cells in floating–cycling under restricted conditions to suppress the degradation by either limiting the charging voltage or the depth of discharge. The cell conditions were occasionally analyzed by non-disassembly analytical methods, which can be performed alternately with the durability tests for multiple times on identical cells. We employed electrochemical impedance spectroscopy (EIS)[26,27] and analysis of the dV/dQ curve derived from low-rate charge–discharge profiles, which have been widely applied to clarify the cell degradation factors such as LLI and LAM.[28,29] To directly capture the status of the electrode materials in the aged cells, neutron diffraction was applied, which utilizes highly penetrating neutrons that can see through commercial LIBs and detect light atoms like lithium and oxygen.[30–34] In addition to *in situ* measurement that has been used to identify the crystal structure changes inside the aged cells,[35] operando neutron diffraction measurement was performed, which allows simultaneous observation of the positive and negative electrodes and offers information on the dynamics of electrode materials during charge–discharge processes, such as reaction inhomogeneity.[36,37] After the cells had experienced significant loss in capacity, they were disassembled to inspect the electrode conditions after degradation.

2 Experimental

2.1 Durability test

Commercially available 18650-type lithium-ion cells (NCR18650B, Panasonic) were used in this study. 8 cells from the same lot were examined to prove their identical charge–discharge behavior as fresh cells, with the initial cell capacity being the same as the value in the manufacturer's catalogue (3.35 Ah). The durability tests were conducted at 25 °C in four floating–cycling modes shown in Table 1, where each cell was 1C discharged once a day, followed by 0.5C charging and then float charging at the designated voltage. Detailed operating conditions are shown in Table S1, which follow the standards described in the cell catalogue sheet. A battery testing system TOSCAT-3000 (Toyo System Co) was used for the durability tests. As shown in Fig. 1(a) and (b), limiting the float charging voltage to 4.0 V and 3.8 V resulted in cell capacities of 2.7 and 2.0 Ah at 1C discharging, which are *ca.* 80% and 60% of the fresh cell capacity (3.35 Ah). Accordingly, the cumulative capacities of the 4.0 V and 3.8 V float-charged cells can be compared to those of fully charged cells with 80% and 60% depth of discharge (DOD). The average discharge voltage differences were *ca.* 0.20 V and 0.35 V, respectively, and had an impact of *ca.* 5–10% on the total energy, as shown in Table 1.

Two sets of durability experiments were conducted, where the cells in four operation modes were set vertically and horizontally. As the degradation behavior was nearly identical (see below), the non-disassembling state-of-health (SOH) analysis, including neutron diffraction, was employed for the vertically set cells. The post-mortem analysis was conducted on the neutron-radiation-free horizontally set cells.

Table 1 Cell capacity, average voltage and energy utilization in each operation mode

Nomenclature	Operation mode	1C capacity/Ah	Average voltage/V	Energy utilization[a]
4.0 V–100%	4.0 V float, 100% DOD	2.7	3.30	0.79
4.2 V–80%	4.2 V float, 80% DOD	2.7	3.50	0.84
3.8 V–100%	3.8 V float, 100% DOD	2.0	3.25	0.58
4.2 V–60%	4.2 V float, 60% DOD	2.0	3.60	0.64

[a] Values relative to the fresh cell capacity of 3.35 Ah with the average voltage of 3.35 V.

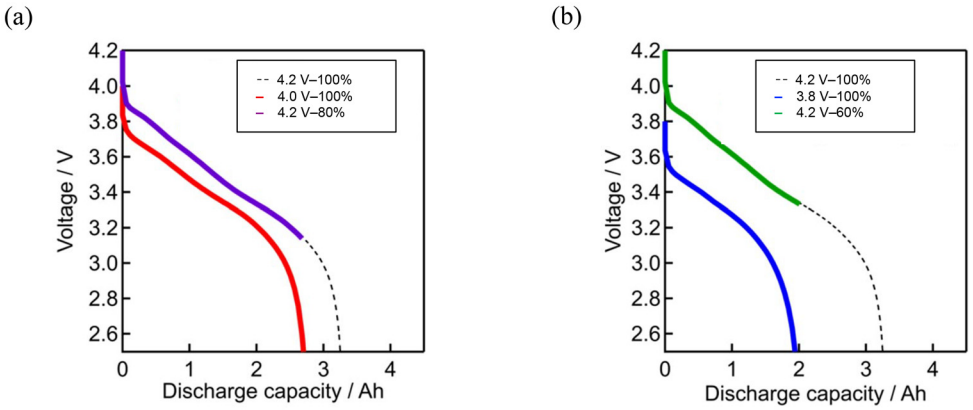

Fig. 1 1C discharge profiles of (a) 4.0 V–100% and 4.2 V–80%, and (b) 3.8 V–100% and 4.2 V–60% DOD cells.

2.2 Electrochemical analysis

The cell SOH was evaluated by charge–discharge curve measurement at a low rate of 0.1C (using TOSCAT-3000, Toyo system) and impedance analysis (using VSP-300, Bio-Logic). The fresh and aged cells were first constant-current (CC) charged at 0.5C at room temperature to a 4.2 V cutoff and then constant-voltage charged at 4.2 V to a 65 mA cutoff. The impedance measurement was conducted at fully charged states in the frequency range of 1 MHz to 5 mHz. Then, the cells were CC discharged at 0.1C to 2.5 V to obtain the discharge profile. The impedance spectra measured at fully discharged states were also obtained but were rather featureless, as shown in the previous study,[24] and were not analyzed in this study. Differential dV/dQ plots *versus* capacity were obtained using the discharge profiles to estimate the degradation mode based on the previous reports.[28,29]

2.3 Operando neutron diffraction analysis

After the electrochemical analysis mentioned above, operando neutron diffraction profiles were obtained to analyze the crystal structure changes of the positive and negative electrode materials during 0.1C discharging to 2.5 V. The diffraction measurements were performed at room temperature using a time-of-flight powder diffractometer at BL-09, called SPICA, at the Materials and Life Science Experimental Facility of the Japan Proton Accelerator Research Complex.[38] Data with statistically sufficient quality for analysis were obtained in 10 minutes. The profiles during the charge and discharge rest periods (under the open-circuit conditions) were also obtained. The detailed neutron measurement conditions have been previously described.[24] The Rietveld refinement using the program Z-Rietveld[39] was employed, assuming that the positive and negative electrodes were $Li_xNi_{0.8}Co_{0.15}Al_{0.05}O_2$ (NCA) and graphite, respectively.[24]

2.4 Post-mortem analysis

A fresh cell and three degraded cells (4.2 V–80%, 4.2 V–60%, 3.8 V–100%, horizontally set) after floating–cycling tests were disassembled in the discharged state under an inert atmosphere. The taken electrodes were washed with dimethyl carbonate and dried. Half-cell tests with metallic lithium as the counter electrode were performed at 1/50C, with the potential ranges from 3.0 V to 4.3 V and 0.005 V to 1.5 V for the layered positive and graphite negative electrodes, respectively, using a charge/discharge device (HJ1001SM8A, Hokuto Denko). The half-cell impedance was measured using a VSP-300 in the frequency range from 1 MHz to 5 mHz at the end of charge. Scanning electron microscopy (SEM) images and elemental mapping of these electrodes by energy-dispersive X-ray spectroscopy (EDS) were obtained using a field emission scanning electron microscope (FE-SEM, Regulus 8230, Hitachi). The cross-section of the positive electrode was prepared using an ion milling system (Ion-Milling System IM4000 PLUS, Hitachi).

3. Results and discussion

3.1 Cell degradation in each operating mode

Fig. 2(a) and (b) show the relative capacity of the vertically set cells at 0.1C *versus* tested days and total discharge capacity, respectively. The cells floated at 4.0 V and 3.8 V exhibited good performance for more than 2 years, with the latter showing superior stability. On the other hand, both cells floated at 4.2 V maintained their SOH at 90% for up to 1 year, and afterward, they degraded, showing much lower capacity retention of less than 60%. The 60% discharged cells lasted longer than the 80% discharged cells, as shown in Fig. 2(a), but the durability was nearly the same based on the total discharge capacity, as shown in Fig. 2(b). These results indicate that controlling the charging voltage is effective in suppressing the degradation, while the depth of discharge is an insignificant factor under the tested conditions.

Nearly the same trends were obtained for the horizontally set cells, as shown in Fig. S1. No significant difference was found between the behavior of the vertically set and horizontally set cells, and the effect of controlling charging voltage is obvious in both cases.

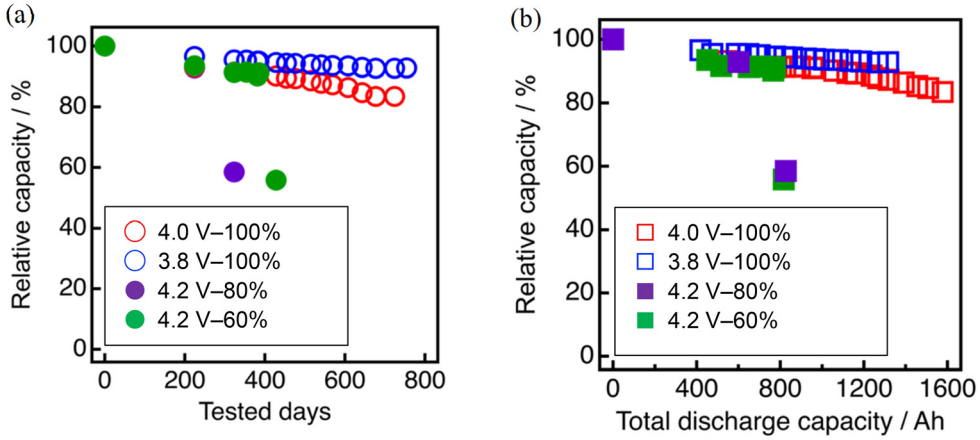

Fig. 2 Relative capacity of the vertically set cells at 0.1C discharge after the durability test *versus* (a) tested days and (b) total discharge capacity (run at 1C).

3.2 Voltage profile analysis

The discharge profiles of the aged cells were analyzed based on the dV/dQ analysis.[28,29] Fig. 3 and 4 show the behavior of the cells that experienced *ca.* 800 Ah of total discharge capacity at 80% and 60% utilization rates, respectively, exhibiting the differences caused by each operation mode.

Fig. 3 shows the comparison of the data of the 4.0 V–100% cell after 354 days and the 4.2 V–80% cell after 323 days, both of which initially showed nearly the same capacity of 3.35 Ah at 0.1C and 2.7 Ah at the 1C rate (see Fig. 1). The 4.0 V–100% cell retained a capacity of 3.0 Ah at the 0.1C rate after 1.3 years of durability testing, and the corresponding dV/dQ profile was nearly maintained. There are characteristic peaks associated

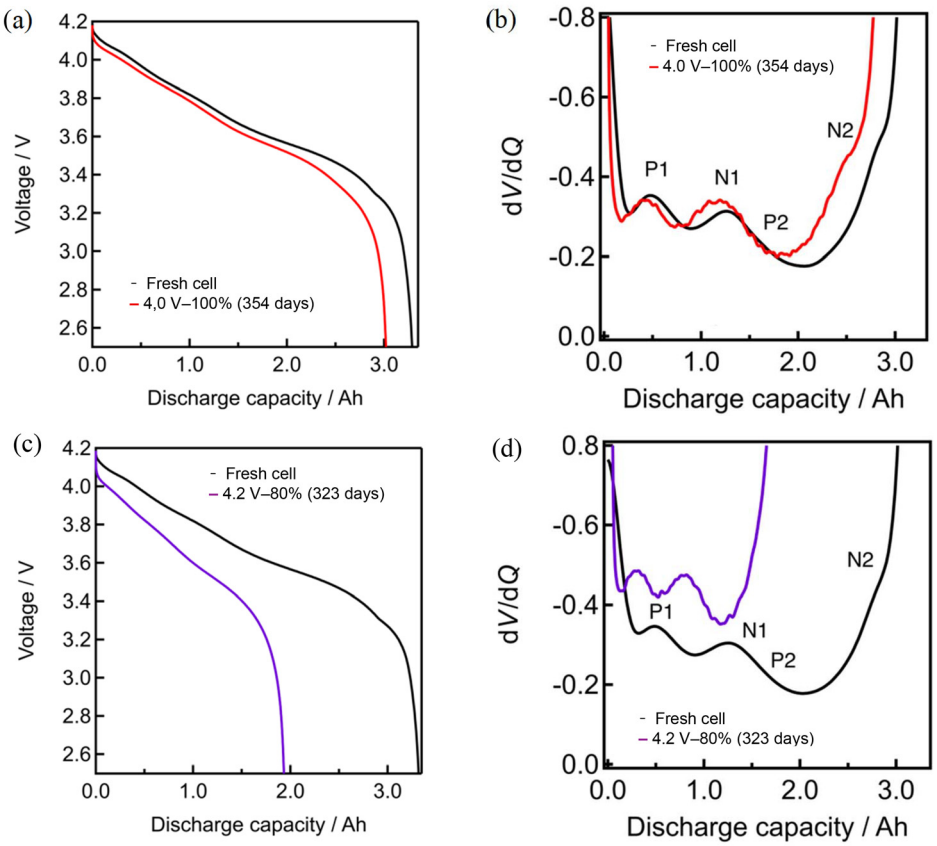

Fig. 3 0.1C discharge profiles and the corresponding dV/dQ profiles of (a and b) 4.0 V–100% (after 354 days) and (c and d) 4.2 V–80% cells (after 323 days). (a) and (c) show the discharge curves, while (b) and (d) show their derivative dV/dQ profiles in comparison with the data of the fresh cell.

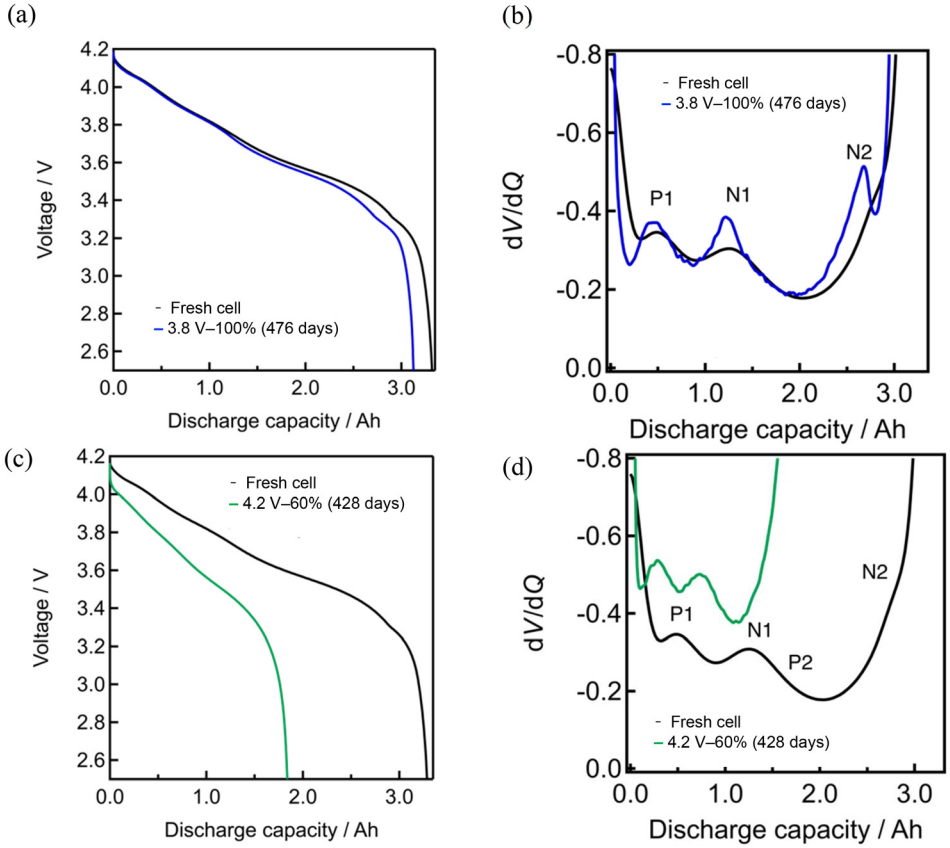

Fig. 4 0.1C discharge profiles and the corresponding dV/dQ profiles of (a and b) 3.8 V–100% (after 476 days) and (c and d) 4.2 V–60% cells (after 428 days). (a) and (c) show discharge curves, while (b) and (d) show their derivative dV/dQ profiles in comparison with the data of the fresh cell.

with the behavior of the positive electrode (P1 and P2) and negative electrode (N1 and N2)[24,40] (see also post-mortem analysis results). Peaks N1 and P2 overlapped in the fresh cells, whereas they became broad and showed the features of N1 and P2 in the aged cell,[28,29,40] indicative of LLI caused by the side reaction at the negative electrode.[41] On the other hand, the 4.2 V–80% cell seriously degraded, showing a capacity of 2.0 Ah at 0.1C. There was a significant voltage drop in the voltage profile as shown in Fig. 3(c), which corresponds to the negatively increased dV/dQ in Fig. 3(d).

Fig. 4 shows the data of the 3.8 V–100% cell after 476 days and the 4.2 V–60% cell after 428 days, which had an initial capacity of 3.35 Ah at 0.1C and 2.0 Ah at the 1C rate (see Fig. 1). The 3.8 V–100% cell exhibited a capacity of 3.1 Ah at 0.1C, with the corresponding dV/dQ profile showing more pronounced peaks than that of the fresh cell, which can be ascribed to the more homogeneous phase transition behavior in the whole electrode caused by the improved electrode wettability during cycling. The 4.2 V–60% cell showed a capacity of only 1.8 Ah at 0.1C, with the dV/dQ profile nearly identical to that of the 4.2 V–80% cell (Fig. 3(d)), again suggesting a minor contribution of the depth of discharge to the cell degradation behavior. The charging voltage limitation was effective in suppressing the significant discharge voltage drop even after 2 years of operation, as shown in Fig. S2.

3.3 Impedance analysis

The impedance analysis was employed to deduce which component had notably changed during the durability test. Our previous study[24] has shown that the high-frequency (at *ca.* 100 Hz) and low-frequency (at *ca.* 0.1 Hz) components correspond to the behavior of the graphite negative and layered positive electrodes, respectively, in accordance with the literature.[42–44] Fig. 5 and 6 show the behavior of the four cells after experiencing *ca.* 800 Ah of total discharge capacity. The semicircles in the 100 Hz region, corresponding to the positive layered electrode, increased with the durability test. The semicircles of the aged cells in Fig. 5 were larger than those in Fig. 6, indicating that high utilization causes impedance growth at the positive electrode. As shown in each figure, limiting the charging voltage is obviously more effective than restricting the depth of discharge. The difference between 4.0 V charging and 3.8 charging is also significant (Fig. S3), showing the importance of limiting charging voltage. It is noted that the intercept corresponding to the ohmic loss decreased in the cells with charging voltage limitation, although its effect on the voltage loss (*ca.* 7 mV at 0.1C) was negligible in the discharge profile. There was little change in the semicircles in the 0.1 Hz region, corresponding to the negative graphite electrode, suggesting that the degradation is mainly caused by the positive electrode.

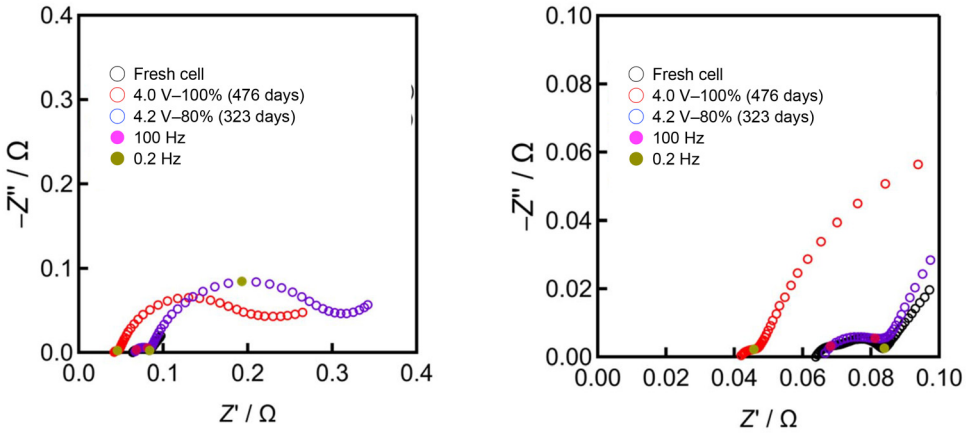

Fig. 5 Nyquist plots of 4.0 V–100% (after 476 days) and 4.2 V–80% (after 323 days) cells at fully charged states with a full view on the left and an enlarged view on the right.

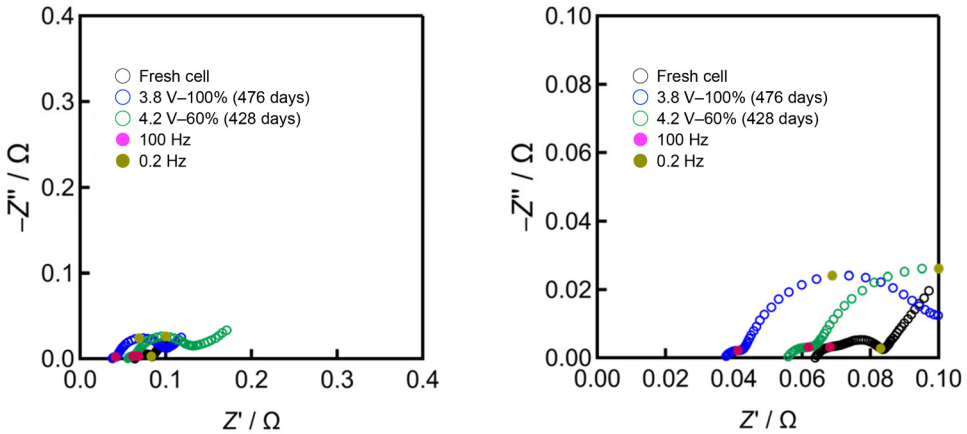

Fig. 6 Nyquist plots of 3.8 V–100% (after 476 days) and 4.2 V–60% (after 428 days) cells at fully charged states, with a full view on the left and an enlarged view on the right.

3.4 Neutron diffraction

The neutron diffraction measurements were performed to clarify the status of the electrode materials in the aged cells after experiencing *ca.* 800 Ah of total discharge capacity. First, *in situ* (no current flow) diffraction profiles were analyzed to know the status before and after discharging.

Fig. S4 shows the profiles of (a) the fresh cell, (b and c) the 80% utilization cells, and (d and e) the 60% utilization cells at the end of charging. With 4.0 V–100% aging, the positive 003 reflection shifted from the pristine 4.716 Å to 4.711 Å,[45] indicative of overcharging, while the enlarged stage 2 peak of graphite suggests that the lithiation level was insufficient, both of which are typical behaviors of LLI. On the other hand, the 4.2 V–80% aged cell had a positive 003 reflection peak shift from the pristine 4.716 Å to 4.720 Å and a very large stage 2 peak of graphite, suggesting insufficient charge in both electrodes. Fig. S5 shows the *in situ* diffraction profiles of these cells at the end of discharging. For the 4.0 V–100% aged cell, although little change was observed on the positive side, the remaining stage 3 and stage 4 peaks indicate captured lithium in the negative electrode. The 4.2 V–80% aged cell showed an increased *d* value on the positive side. On the negative side, a strong stage 2 peak and even a stage 1 peak of graphite were observed. This suggests that lithium insertion into the positive electrode during discharging was seriously interfered, owing to the RIPE degradation. The same trends were observed in the 60% utilization cells, although the degree of degradation was less significant. The 3.8 V–100% aged cell showed nearly identical profiles to the fresh cell, showing minimum degradation, thanks to the limited charging voltage. The overcharged status of the positive 003 reflection suggests that the main degradation mode is LLI. The 4.2 V–60% aged cell showed a strong stage 2 peak of graphite (without a stage 1 peak) at the end of discharging, implying that the lithium insertion into the positive electrode was impeded during discharging.

Fig. 7 represents the operando neutron diffraction profiles of the 80% utilization cells during discharging at 0.1C. The

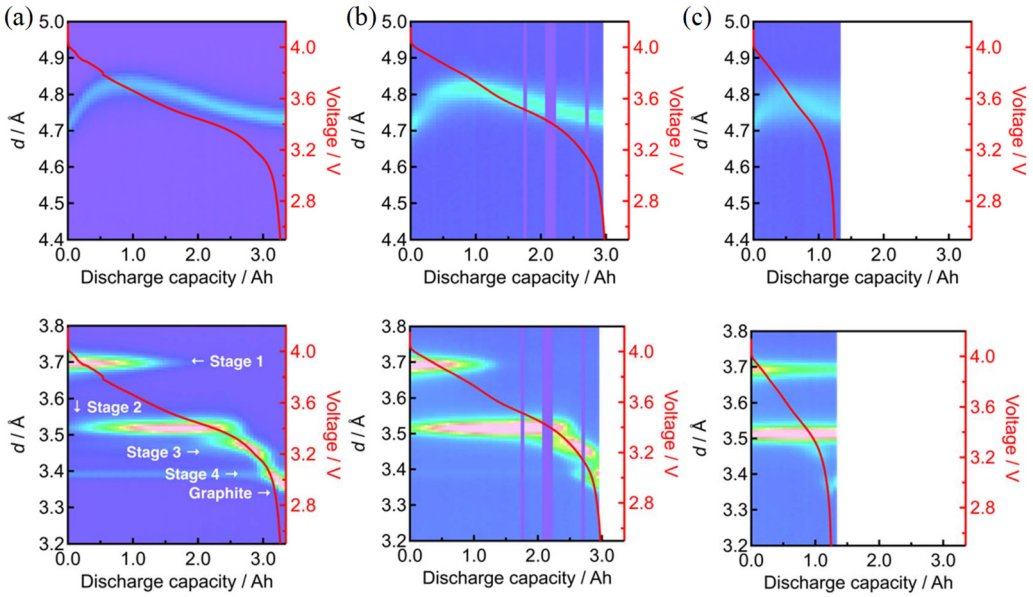

Fig. 7 Operando neutron diffraction profiles of (a) the fresh cell and (b) 4.0 V–100% (after 476 days) and (c) 4.2 V–80% (after 323 days) aged cells during discharging at 0.1C. The layered positive 003 and negative graphite 00*l* reflections are shown on the upper and lower sides, respectively.

occasional loss of diffraction signals was caused by the incident neutron beam interruption. When compared to the fresh cell behavior, the aged cells, in particular the 4.2 V–80% cell, showed broadened profiles on the positive side. This implies a reaction distribution caused by a spatially inhomogeneous resistance increase in the electrode.[24] It is also noted that the state of charge (SOC) of the negative graphite electrode is severely limited in the 4.2 V–80% cell, while the SOC shift of the positive electrode is not so significant. This can be ascribed to a relative shift in their potential windows, which is typically seen in LLI-aged cells.[29] As shown in Fig. 8, the cells with 60% utilization showed the same trends as the 80% utilization cells, although the degree of profile broadening and capacity loss was somewhat mitigated.

Fig. S6 and S7 present the results of the Rietveld refinement (lattice constants *a*, *c*, *c*/*a* and cell volume) for the 4.0 V–100% and 3.8 V–100% aged cells, respectively. Although the lattice constant *c* of the fresh cell was inadequately evaluated (too

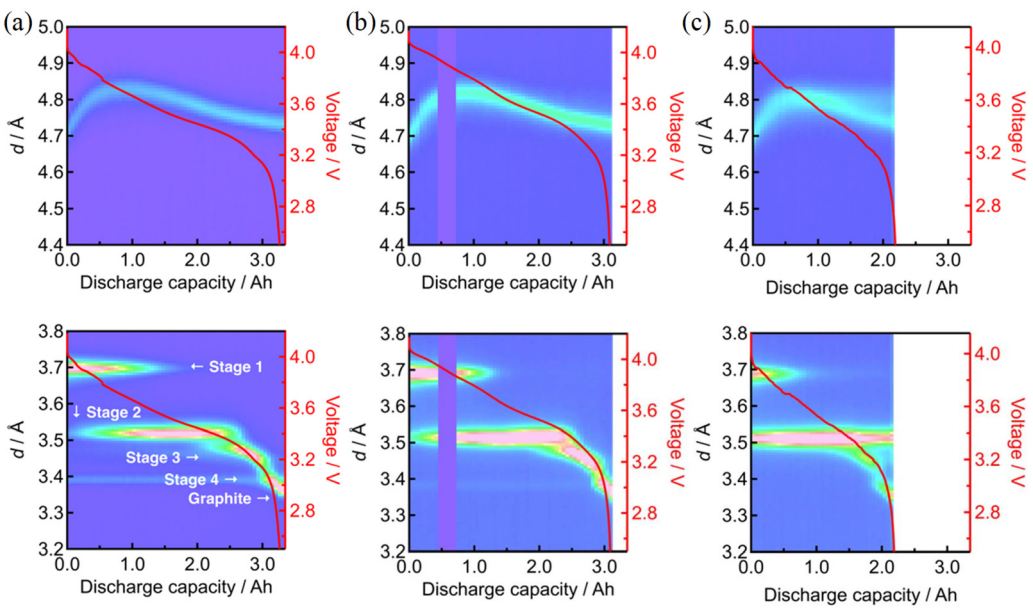

Fig. 8 Operando neutron diffraction profiles of (a) the fresh cell and (b) 3.8 V–100% (after 476 days) and (c) 4.2 V–60% (after 428 days) aged cells during discharging at 0.1C. The layered positive 003 and negative graphite 00*l* reflections are shown on the upper and lower sides, respectively.

long) due to the unreliable background data in neutron diffraction measurements, it turns out from the changes of the reliable lattice constant a that there was some loss of active materials (profile shrinkage along the horizontal axis) in the 4.0 V–100% aged cells, while nearly no degradation occurs in the 3.8 V–100% aged cells. The main difference of the two is that the 4.0 V–100% aged cell undergoes interlayer distance (c/3) shrinkage at the end of charging, while the 3.8 V–100% aged cell experiences nearly no interlayer distance shrinkage. It is deduced that the repeated lattice expansion and shrinkage in the 4.0 V–100% aged cell leads to the formation of microcracks (see below), causing the loss of active materials. The refinement of the 4.2 V–80% and 4.2 V–60% aged cells did not converge because of the significantly broadened diffraction profiles caused by reaction inhomogeneity.

As the positive 003 profile broadening differs from sample to sample, as shown in Fig. S8, the profiles were quantitatively analyzed using Gaussian fitting to obtain the full width at half maximum (FWHM) values, as shown in Fig. 9. Good fits were generally obtained, although the values at the beginning of discharging were scattered due to large d value changes. The FWHM values for the 4.0 V–100% and 3.8 V–100% cells were nearly the same as that for the fresh cell, showing the positive effect of charging voltage limitation. On the other hand, those for the 4.2 V–80% and 4.2 V–60% cells were comparatively high, showing the loss of crystallinity or microcrack evolution in the layered positive electrode material.[35] The FWHM value change in the course of discharging suggests that the reaction distribution caused by the inhomogeneous resistance increase also affected the behavior. Because such reaction inhomogeneity is generally lost during cell relaxation, these results show the advantages of the operando analysis.[24,36,37]

3.5 Post-mortem analysis

Post-mortem analysis was employed to directly inspect the status of aged electrodes. Since the neutron-irradiated LIB cells are not applicable for disassembly, we used other cells that had been similarly tested (horizontally set). Although the final cell conditions shown in Table 2 were different from those described above, the nearly identical degradation behavior shown in Fig. 2 and S1 suggests that the analysis results shown below are well applicable to the cells described above. The 3.8 V–100% cell was disassembled after experiencing a total capacity that is 1.5–1.8 times greater than that of the

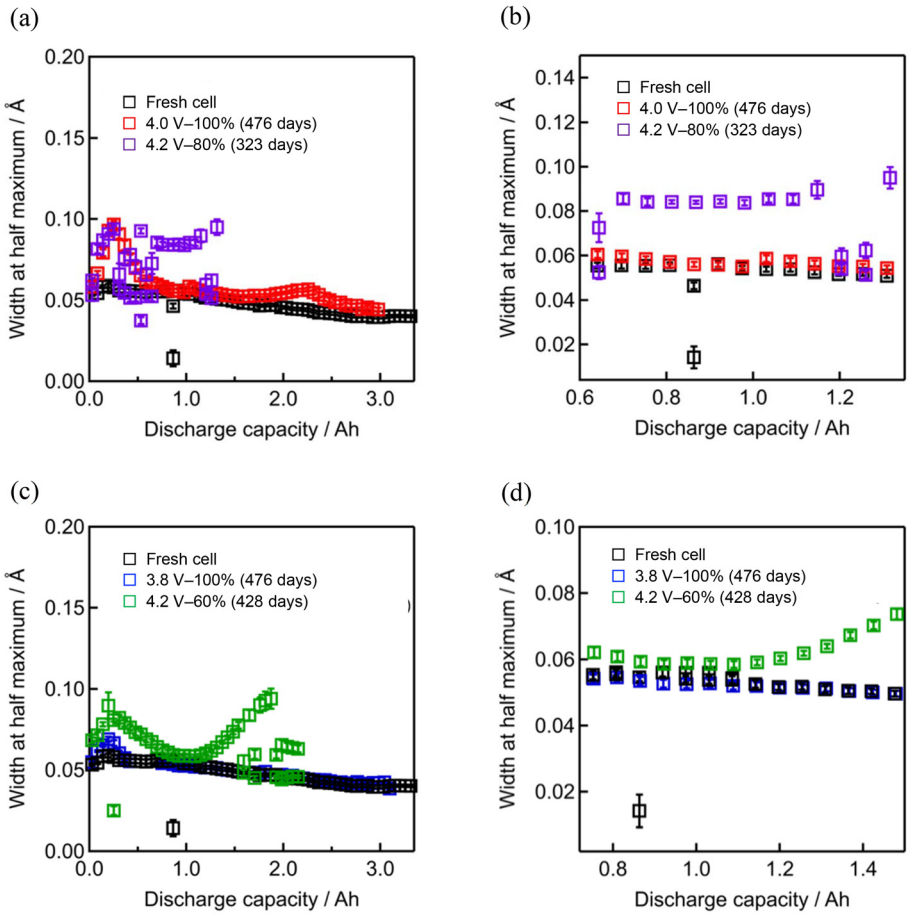

Fig. 9 Full width at half maximum of layered positive 003 reflection obtained during operando neutron diffraction at 0.1C. (a and b) 4.0 V–100% after 476 days and 4.2 V–80% after 323 days; (c and d) 3.8 V–100% after 476 days and 4.2 V–60% after 428 days. (b) and (d) show the enlarged view of (a) and (c), respectively.

Table 2 Tested days, total discharge capacity and discharge capacity at 0.1C of LIBs before cell disassembly, and discharge capacity of the disassembled positive and negative electrodes tested in half cells at 0.02C

Tested mode	Tested days	Total discharge capacity/Ah	Discharge capacity of LIBs before cell disassembly/Ah	Disassembled positive electrode capacity/mAh	Disassembled negative electrode capacity/mAh
Fresh cell	—	—	3.35	5.43	8.13
4.2 V–80%	334	764	1.20 (−64.2%)	3.87 (−28.7%)	7.76 (−4.6%)
4.2 V–60%	334	661	2.59 (−22.7%)	4.65 (−14.4%)	
3.8 V–100%	636	1178	3.13 (−6.6%)	4.73 (−12.9%)	6.69 (−17.7%)

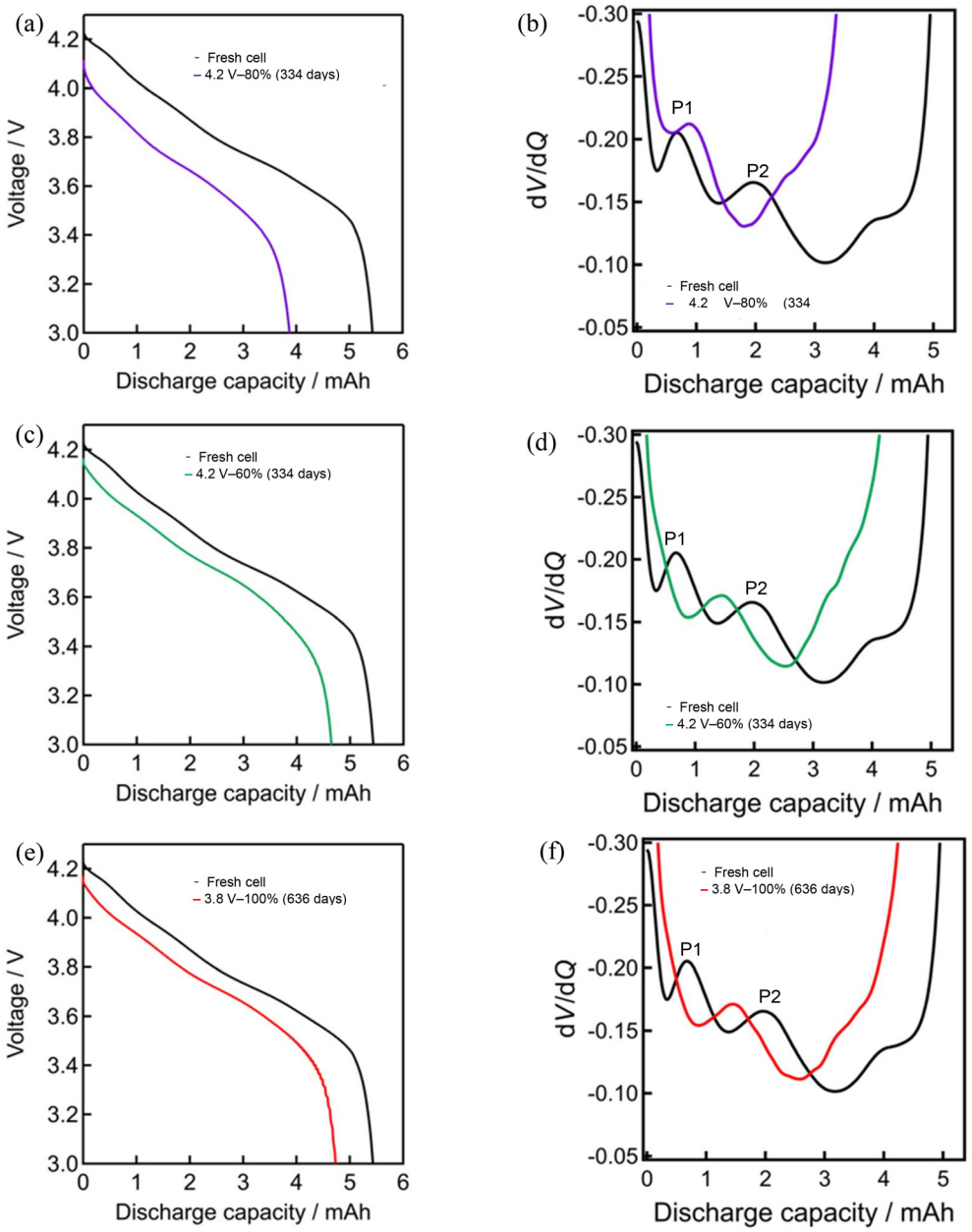

Fig. 10 Discharge profiles of positive electrodes in half cells at 0.02C derived from (a and b) 4.2 V–80%, (c and d) 4.2 V–60%, (e and f) 3.8 V–100% cells. (a), (c) and (e) show the discharge curves, while (b), (d) and (f) show their derivative dV/dQ profiles in comparison with the data of the fresh cell. Peaks P1 and P2 show the same transitions as those shown in Fig. 3 and 4.

other two cells in order to clarify how the degradation proceeded under the most moderate condition.

Fig. 10 presents the behavior of the positive electrodes taken out from the aged cells. The 4.2 V–80% electrode shows a large voltage loss, which is similar to that in the full cell shown in Fig. 3(c). In contrast, the 4.2 V–60% and 3.8 V–100% electrodes showed limited degradation. Fig. 11 shows the data of the negative electrodes taken out from the aged cells. The data for the 4.2 V–60% cell were not available due to the fragile nature of the electrode film. It is noteworthy that the graphite electrode taken from the most degraded 4.2 V–80% LIB was hardly degraded, as shown in Fig. 11(a) and (b). This clearly indicates that the positive electrode degradation mainly led to full cell deterioration. Note that the original LIB capacity loss was much greater than that of the electrode degradation shown in Fig. 10(a) (see also Table 2). Other factors such as electrolyte depletion could cause serious capacity loss in LIBs.

From the EIS results shown in Fig. 12, an increase in the positive electrode impedance is clearly seen in the 4.2 V charged cells, while some increase in the negative electrode impedance is observed in the 3.8 V charged cell. Considering that the 3.8 V charged cell had delivered much higher capacity than the two 4.2 V charged cells, it is suggested that the RIPE degradation proceeds faster than the LLI degradation, leading to apparently insignificant LLI degradation in the 4.2 V charged cells. Actually, some RIPE degradation seems to proceed also in the 3.8 V charged cell in the long run, as shown in Fig. 6 and 10(e), although the charging voltage restriction is indeed effective for RIPE suppression.

Fig. 13 shows the SEM and EDS (fluorine) analysis results of the positive electrode derived from LIB full cells. When compared to the fresh state, the aged electrodes suffered from cracking with fluorine signals, as observed in the previous study,[24] which seems to be responsible for the increased impedance and the voltage loss. Fig. S9 shows the SEM-only, EDS-only and the overlapped images of the particles derived from 4.2 V–60% and 3.8 V–100% aged cells, taken in addition to those in Fig. 13. These images clarified that the fluorine signals were observed everywhere in the particles taken from the 4.2 V–60% aged cell, while the signals were mainly located in between the secondary particles taken from the 3.8 V–100% aged cell, suggesting the significant formation of microcracks (even if invisible in the SEM images) in the former.

Fig. 14 shows the SEM and EDS results of the negative electrode. The fluorine content in the 3.8 V–100% electrode was nearly the same as the fresh electrode, while much thicker

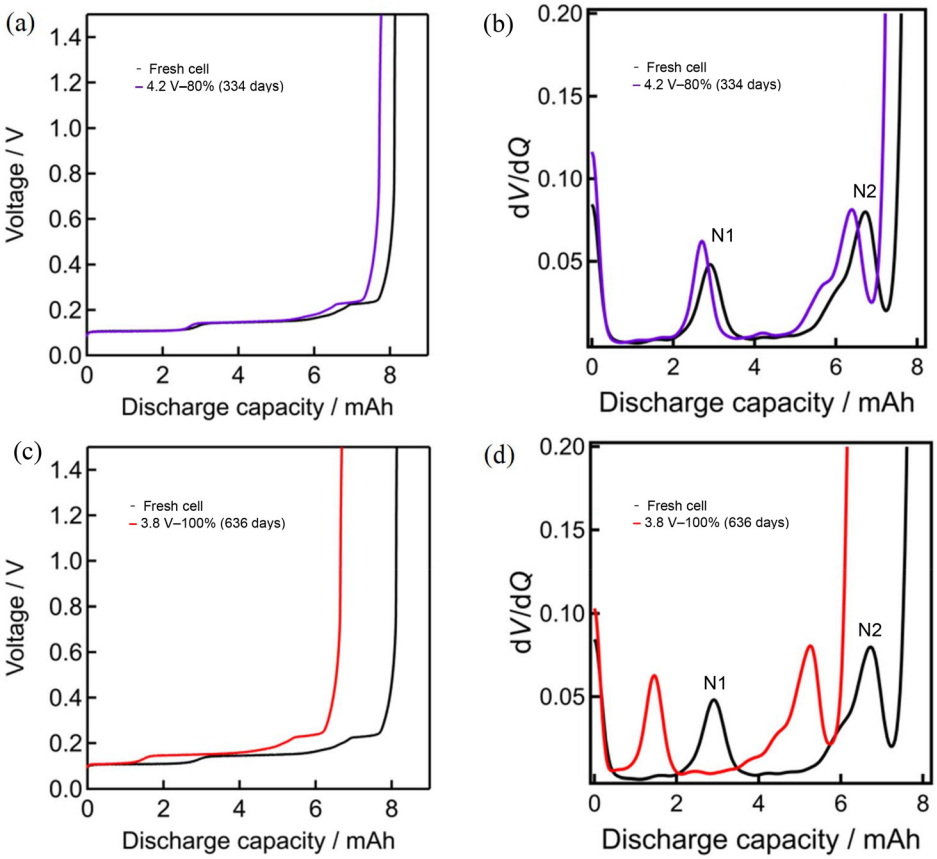

Fig. 11 Discharge profiles of negative electrodes in half cells at 0.02C derived from (a and b) 4.2 V–80% and (c and d) 3.8 V–100% cells. (a) and (c) show the discharge curves, while (b) and (d) show their derivative d*V*/d*Q* profiles in comparison with the data of the fresh cell. Peaks N1 and N2 show the same transitions as those shown in Fig. 3 and 4.

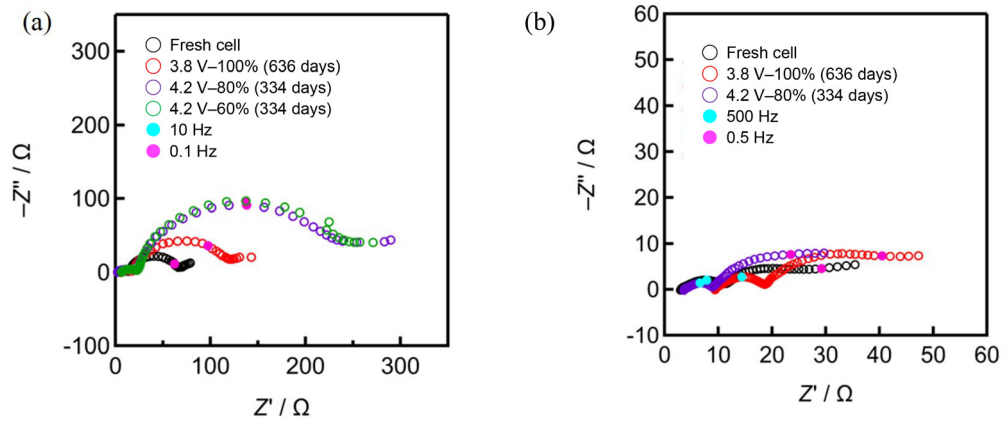

Fig. 12 Nyquist plots of the (a) positive and (b) negative electrodes derived from aged LIBs tested in lithium half cells in fully charged states.

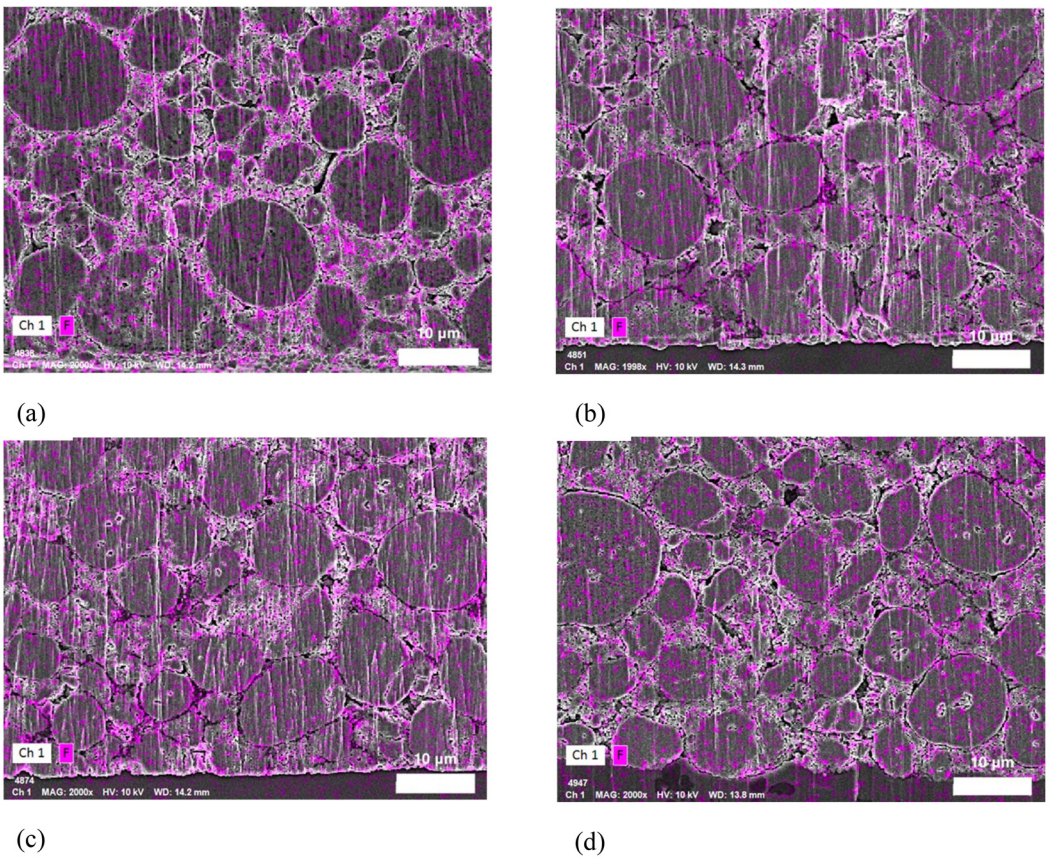

Fig. 13 Fluorine mapping in the cross-section of the positive electrodes derived from the (a) fresh cell and (b) 4.2 V–100%, (c) 4.2 V–60% and (d) 3.8 V–100% aged cells.

fluorine-containing films were formed in the 4.2 V–80% and 4.2 V–60% electrodes. On the other hand, the graphite electrode derived from the 4.2 V–80% (after 334 days) cell was in a high SOH, as shown in Fig. 11 and 12. This suggests that the film formation was insignificantly detrimental to the negative electrode behavior under the tested conditions.

3.6 Effect of voltage limitation

Here, we discuss how the voltage limitation affects the status of the materials and leads to the suppression of the degradation. While the detailed high-resolution *ex situ* analysis of the resistive film should be effective, the significant degra-

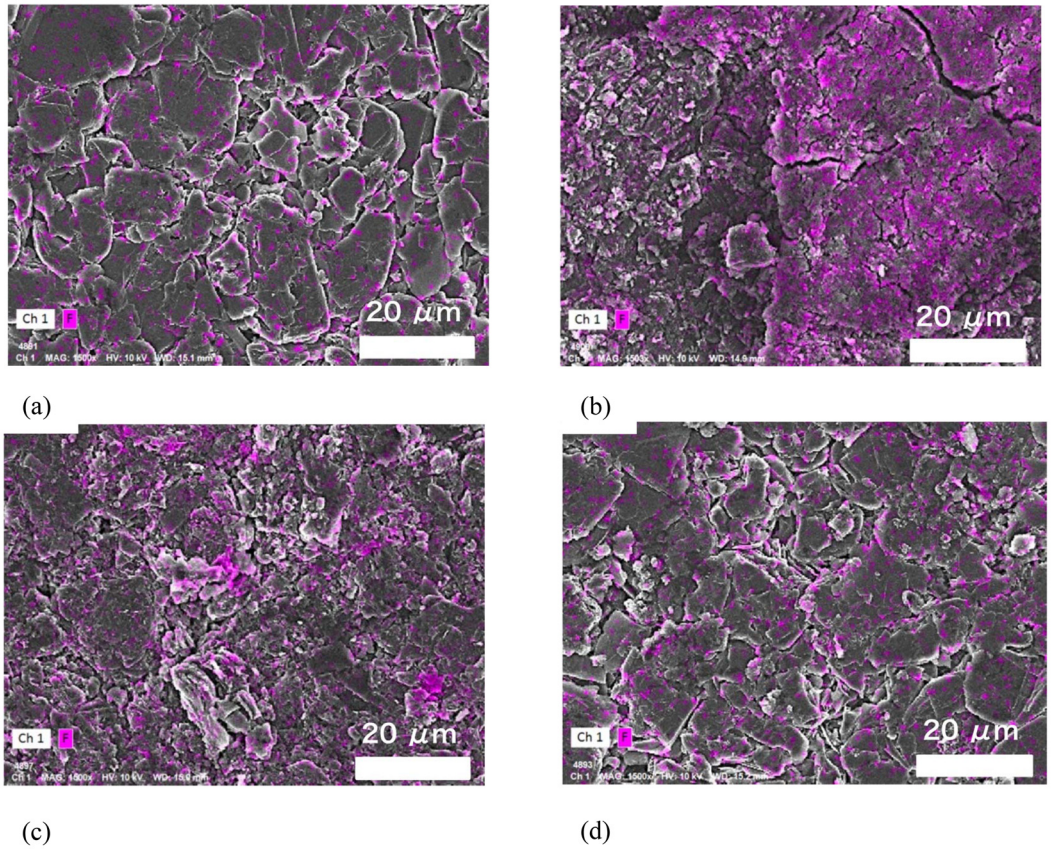

Fig. 14 Fluorine mapping at the surface of the negative electrodes derived from the (a) fresh cell and (b) 4.2 V–80%, (c) 4.2 V–60% and (d) 3.8 V–100% aged cells.

dation inhomogeneity occurring in 20 grams of positive electrode materials (3.4 Ah divided by 170 mAh g^{-1}) seems to be incompatible with high-space resolution analysis. Therefore, we here discuss the possible effect of voltage limitation using rather macroscopic data of neutron diffraction. As shown in Fig. 7, the limitation of the upper voltage (4.0 and 3.8 V instead of 4.2 V) was effective in suppressing the diffraction profile broadening of the positive electrode. This broadening is caused by the reaction inhomogeneity and such reaction inhomogeneity should be derived from the formation of spatially inhomogeneous resistive films on the positive electrode particles.[24] The oxidative resistive film (so-called cathode-electrolyte interphase CEI) formation on the positive electrode is usually insignificant in the voltage region of below 4.2 V,[46,47] while the formation of graphite stage 1, causing the reductive resistive film (so-called solid-electrolyte interphase SEI),[48] is suppressed by lowering the voltage limit. In addition, the results of the Rietveld refinement shown in Fig. S6 and 7 indicate that the limitation of the upper voltage is effective in avoiding the shrinkage of the interlayer (lattice constant *c*) and hence the formation of microcracks in the positive electrode particles at the end of charging, as suggested from Fig. S9. By considering the cross-talk effect indicating the effect of the negative electrode film on the positive electrode degradation,[49–52] we deduce that the voltage limitation is effective in suppressing both SEI formation and microcrack formation at the positive electrode, resulting in the restriction of RIPE. Further studies are needed to clarify which is mainly responsible to the RIPE degradation, the positive electrode particle cracking by the significant volume change in the high SOC region or the formation of the resistive film associated with high voltage charging, which would be attained by experiments using other electrode materials.

4. Conclusions

This paper reveals that the serious capacity fade occurring in the floating–cycling mode can be mitigated by restricting the charging voltage. The operando neutron diffraction, voltage curve and impedance analyses, as well as post-mortem analysis, indicate that the RIPE degradation as the main origin of degradation is alleviated with the charging voltage limitation rather than the depth of discharge limitation. Such a resistance increase affects the dynamics of the reaction inhomogeneity of the electrode, as represented by broadening diffraction lines in neutron analysis. The film formation on the microcracks in the positive electrode leads to the resistance

increase in the floating–cycling mode, and charging voltage limitation is effective in mitigating both of the degradation origins. The results found in this study will give insights into the capacity loss in the LIBs and contribute to the LIB life extension. Further studies to clarify the film formation mechanism are expected to extend the cell life in the floating–cycling mode, which in turn can enhance the facility utilization of the backup batteries.

Conflicts of interest

There are no conflicts to declare.

Data availability

The data supporting this article have been included as part of the SI.

Supplementary information is available. See DOI: **https://doi.org/10.1039/d5eb00096c**.

Acknowledgements

This work was financially supported by NTT Facilities Inc. The neutron scattering experiments were approved by the Neutron Scattering Program Advisory Committee of IMSS, KEK (Proposal No. 2018L0301 and 2019S10). The authors acknowledge support from Dr Naomi Inazu for SEM/EDS observation.

References

1 B. Diouf and R. Pode, Potential of lithium-ion batteries in renewable energy, *Renewable Energy*, 2015, **76**, 375–380, DOI: **10.1016/j.renene.2014.11.058**.

2 T. Iwahori, I. Mitsuishi, S. Shiraga, N. Nakajima, H. Momose, Y. Ozaki, S. Taniguchi, H. Awata, T. Ono and K. Takeuchi, Development of lithium ion and lithium polymer batteries for electric vehicle and home-use load leveling system application, *Electrochim. Acta*, 2000, **45**, 1509–1512, DOI: **10.1016/S0013-4686(99)00366-7**.

3 K. Richa, C. W. Babbitt, N. G. Nenadic and G. Gaustad, Environmental trade-offs across cascading lithium-ion battery life cycles, *Int. J. Life Cycle Assess.*, 2017, **22**, 66–81, DOI: **10.1007/s11367-015-0942-3**.

4 N. Takami, H. Inagaki, Y. Tatebayashi, H. Saruwatari, K. Honda and S. Egusa, High-power and long-life lithium-ion batteries using lithium titanium oxide anode for automotive and stationary power applications, *J. Power Sources*, 2013, **244**, 469–475, DOI: **10.1016/j.jpowsour.2012.11.055**.

5 C. P. Grey and J. M. Tarascon, Sustainability and in situ monitoring in battery development, *Nat. Mater.*, 2017, **16**, 45–56, DOI: **10.1038/NMAT4777**.

6 F. H. Gandoman, J. Jaguemont, S. Goutam, R. Gopalakrishnan, Y. Firouz, T. Kalogiannis, N. Omar and J. Van Mierlo, Concept of reliability and safety assessment of lithium-ion batteries in electric vehicles: Basics, progress, and challenges, *Appl. Energy*, 2019, **251**, 113343, DOI: **10.1016/j.apenergy.2019.113343**.

7 L. S. de Vasconcelos, R. Xu, Z. R. Xu, J. Zhang, N. Sharma, S. R. Shah, J. X. Han, X. M. He, X. Y. Wu, H. Sun, S. Hu, M. Perrin, X. K. Wang, Y. J. Liu, F. Lin, Y. Cui and K. J. Zhao, Chemomechanics of Rechargeable Batteries: Status, Theories, and Perspectives, *Chem. Rev.*, 2022, **122**, 13043–13107, DOI: **10.1021/acs.chemrev.2c00002**.

8 Y. H. Che, X. S. Hu, X. K. Lin, J. Guo and R. Teodorescu, Health prognostics for lithium-ion batteries: mechanisms, methods, and prospects, *Energy Environ. Sci.*, 2023, **16**, 338–371, DOI: **10.1039/d2ee03019e**.

9 K. Jia, G. R. Yang, Y. J. He, Z. J. Cao, J. T. Gao, H. Y. Zhao, Z. H. Piao, J. X. Wang, A. M. Abdelkader, Z. Liang, R. V. Kumar, G. M. Zhou, S. J. Ding and K. Xi, Degradation Mechanisms of Electrodes Promotes Direct Regeneration of Spent Li-Ion Batteries: A Review, *Adv. Mater.*, 2024, **36**, 2313273, DOI: **10.1002/adma.202313273**.

10 C. R. Birkl, M. R. Roberts, E. McTurk, P. G. Bruce and D. A. Howey, Degradation diagnostics for lithium ion cells, *J. Power Sources*, 2017, **341**, 373–386, DOI: **10.1016/j.jpowsour.2016.12.011**.

11 J. Vetter, P. Novák, M. R. Wagner, C. Veit, K. C. Möller, J. O. Besenhard, M. Winter, M. W. Mehrens, C. Vogler and A. Hammouche, Ageing mechanisms in lithium-ion batteries, *J. Power Sources*, 2005, **147**, 269–281, DOI: **10.1016/j.jpowsour.2005.01.006**.

12 M. Wohlfahrt-Mehrens, C. Vogler and J. Garche, Aging mechanisms of lithium cathode materials, *J. Power Sources*, 2004, **127**, 58–64, DOI: **10.1016/j.jpowsour.2003.09.034**.

13 T. Yoshida, M. Takahashi, S. Morikawa, C. Ihara, H. Katsukawa, T. Shiratsuchi and J. Yamaki, Degradation Mechanism and Life Prediction of Lithium-Ion Batteries, *J. Electrochem. Soc.*, 2006, **153**(3), A576–A582, DOI: **10.1149/1.2162467**.

14 P. Verma, P. Maire and P. Novák, A review of the features and analyses of the solid electrolyte interphase in Li-ion batteries, *Electrochim. Acta*, 2010, **55**, 6332–6341, DOI: **10.1016/j.electacta.2010.05.072**.

15 K. Kleiner and H. Ehrenberg, Challenges Considering the Degradation of Cell Components in Commercial Lithium-Ion Cells: A Review and Evaluation of Present Systems, *Top. Curr. Chem.*, 2017, **375**, 1–45, DOI: **10.1007/s41061-017-0139-2**.

16 C. Kupper, B. Weißhar, S. Rißmann and W. G. Bessler, End-of-Life Prediction of a Lithium-Ion Battery Cell Based on Mechanistic Aging Models of the Graphite Electrode, *J. Electrochem. Soc.*, 2018, **165**(14), A3468–A3480, DOI: **10.1149/2.0941814jes**.

17 B. P. Matadi, S. Geniès, A. Delaille, T. Waldmann, M. Kasper, M. W. Mehrens, F. Aguesse, E. Bekaert, I. J. Gordon, L. Daniel, X. Fleury, M. Bardet, J. F. Martin and Y. Bultel, Effects of Biphenyl Polymerization on Lithium Deposition in Commercial Graphite/NMC Lithium-Ion Pouch-Cells during Calendar Aging at High

Temperature, *J. Electrochem. Soc.*, 2017, **164**(6), A1089–A1097, DOI: 10.1149/2.0631706jes.

18 Z. Mao, M. Farkhondeh, M. Pritzker, M. Fowler and Z. Chen, Calendar Aging and Gas Generation in Commercial Graphite/NMC-LMO Lithium-Ion Pouch Cell, *J. Electrochem. Soc.*, 2017, **164**(14), A3469–A3483, DOI: 10.1149/2.0241714jes.

19 V. Agubra and J. Fergus, Lithium ion battery anode aging mechanisms, *Materials*, 2013, **6**, 1310–1325, DOI: 10.3390/ma6041310.

20 M. Dollé, L. Sannier, B. Beaudoin, M. Trentin and J. M. Tarascon, Live scanning electron microscope observations of dendritic growth in lithium/polymer cells, *Electrochem. Solid-State Lett.*, 2002, **5**(12), A286–A289, DOI: 10.1149/1.1519970.

21 J. Li, J. Harlow, N. Stakheiko, N. Zhang, J. Paulsen and J. Dahn, Dependence of Cell Failure on Cut-Off Voltage Ranges and Observation of Kinetic Hindrance in $LiNi_{0.8}Co_{0.15}Al_{0.05}O_2$, *J. Electrochem. Soc.*, 2018, **165**(11), A2682–A2695, DOI: 10.1149/2.0491811jes.

22 S. Watanabe, M. Kinoshita, T. Hosokawa, K. Morigaki and K. Nakura, Capacity fade of $LiAl_yNi_{1-x-y}Co_xO_2$ cathode for lithium-ion batteries during accelerated calendar and cycle life tests (surface analysis of $LiAl_yNi_{1-x-y}Co_xO_2$ cathode after cycle tests in restricted depth of discharge ranges), *J. Power Sources*, 2014, **258**, 210–217, DOI: 10.1016/j.jpowsour.2014.02.018.

23 J. Wang, H. Kim, H. Hyun, S. Jo, J. Han, D. Ko, S. Seo, J. Kim, H. Kong and J. Lim, Probing and Resolving the Heterogeneous Degradation of Nickel–Rich Layered Oxide Cathodes across Multi–Length Scales, *Small Methods*, 2020, **4**, 2000551, DOI: 10.1002/smtd.202000551.

24 T. Omiya, A. Ikezawa, K. Takahashi, K. Saito, M. Yonemura, T. Saito, T. Kamiyama, K. Mori and H. Arai, Combination of float charging and occasional discharging to cause serious LIB degradation analyzed by operando neutron diffraction, *Energy Adv.*, 2024, **3**, 529–542, DOI: 10.1039/d3ya00557g.

25 T. Tsujikawa, K. Yabuta, T. Matsushita, M. Arakawa and K. Hayashi, A Study on the Cause of Deterioration in Float-Charged Lithium-Ion Batteries Using $LiMn_2O_4$ as a Cathode Active Material, *J. Electrochem. Soc.*, 2011, **158**(3), A322–A325, DOI: 10.1149/1.3543651.

26 A. Barai, K. Uddin, M. Dubarry, L. Somerville, A. McGordon, P. Jennings and I. Bloom, A comparison of methodologies for the non-invasive characterisation of commercial Li-ion cells, *Prog. Energy Combust. Sci.*, 2019, **72**, 1–31, DOI: 10.1016/j.pecs.2019.01.001.

27 N. Meddings, M. Heinrich, F. Overney, J. S. Lee, V. Ruiz, E. Napolitano, S. Seitz, G. Hinds, R. Raccichini, M. Gabers and J. Park, Application of electrochemical impedance spectroscopy to commercial Li-ion cells: A review, *J. Power Sources*, 2020, **480**, 228742, DOI: 10.1016/j.jpowsour.2020.228742.

28 I. Bloom, A. N. Jansen, D. P. Abraham, J. Knuth, S. A. Jones, V. S. Battaglia and G. L. Henriksen, Differential voltage analyses of high-power, lithium-ion cells 1. Technique and application, *J. Power Sources*, 2005, **139**, 295–303, DOI: 10.1016/j.jpowsour.2004.07.021.

29 K. Honkura and T. Horiba, Study of the deterioration mechanism of $LiCoO_2$/graphite cells in charge/discharge cycles using the discharge curve analysis, *J. Power Sources*, 2014, **264**, 140–146, DOI: 10.1016/j.jpowsour.2014.04.036.

30 F. Rosciano, M. Holzapfel, W. Scheifele and P. Novák, A novel electrochemical cell for in situ neutron diffraction studies of electrode materials for lithium-ion batteries research papers, *J. Appl. Crystallogr.*, 2008, **41**, 690–694, DOI: 10.1107/S0021889808018025.

31 H. Berg, H. Rundlöv and J. O. Thomas, The $LiMn_2O_4$ to λ-MnO_2 phase transition studied by in situ neutron diffraction, *Solid State Ionics*, 2001, **144**, 65–69, DOI: 10.1016/S0167-2738(01)00894-3.

32 A. Senyshyn, O. Dolotko, M. J. Mühlbauer, K. Nikolowski, H. Fuess and H. Ehrenberg, Lithium Intercalation into Graphitic Carbons Revisited: Experimental Evidence for Twisted Bilayer Behavior, *J. Electrochem. Soc.*, 2013, **160**, A3198–A3205, DOI: 10.1149/2.031305jes.

33 N. Sharma, V. K. Peterson, M. M. Elcombe, M. Avdeev, A. J. Studer, N. Blagojevic, R. Yusoff and N. Kamarulzaman, Structural changes in a commercial lithium-ion battery during electrochemical cycling: An in situ neutron diffraction study, *J. Power Sources*, 2010, **195**, 8258–8266, DOI: 10.1016/j.jpowsour.2010.06.114.

34 D. Petz, V. Baran, C. Peschel, M. Winter, S. Nowak, M. Hofmann, R. Kostecki, R. Niewa, M. Bauer, P. M. Buschbaum and A. Senyshyn, Aging-Driven Composition and Distribution Changes of Electrolyte and Graphite Anode in 18650-Type Li-Ion Batteries, *Adv. Energy Mater.*, 2022, **12**, 2201652, DOI: 10.1002/aenm.202201652.

35 N. Paul, N. Paula, J. Keil, F. M. Kindermann, S. Schebesta, O. Dolotko, M. J. Mühlbauer, L. Kraft, S. V. Erhard, A. Jossen and R. Gilles, Aging in 18650-type Li-ion cells examined with neutron diffraction, electrochemical analysis and physico-chemical modeling, *J. Energy Storage*, 2018, **17**, 383–394, DOI: 10.1016/j.est.2018.03.016.

36 S. Taminato, M. Yonemura, S. Shiotani, T. Kamiyama, S. Torii, M. Nagao, Y. Ishikawa, K. Mori, T. Fukunaga, Y. Onodera, T. Naka, M. Morishima, Y. Ukyo, D. S. Adipranoto, H. Arai, Y. Uchimoto, Z. Ogumi, K. Suzuki, M. Hirayama and R. Kanno, Real-time observations of lithium battery reactions - Operando neutron diffraction analysis during practical operation, *Sci. Rep.*, 2016, **6**, 28843, DOI: 10.1038/srep28843.

37 S. Shiotani, T. Naka, M. Morishima, M. Yonemura, T. Kamiyama, Y. Ishikawa, Y. Ukyo, Y. Uchimoto and Z. Ogumi, Degradation analysis of 18650-type lithium-ion cells by operando neutron diffraction, *J. Power Sources*, 2016, **325**, 404–409, DOI: 10.1016/j.jpowsour.2016.06.026.

38 M. Yonemura, K. Mori, T. Kamiyama, T. Fukunaga, S. Torii, M. Nagao, Y. Ishikawa, Y. Onodera, D. S. Adipranoto, H. Arai, Y. Uchimoto and Z. Ogumi, Development of SPICA, new dedicated neutron powder diffractometer for battery

studies, *J. Phys.: Conf. Ser.*, 2014, **502**, 012053, DOI: 10.1088/1742-6596/502/1/012053.

39 R. Oishi, M. Yonemura, Y. Nishimaki, S. Torii, A. Hoshikawa, T. Ishigaki, T. Morishima, K. Mori and T. Kamiyama, Rietveld analysis software for J-PARC, *Nucl. Instrum. Methods Phys. Res., Sect. A*, 2009, **600**, 94–96, DOI: 10.1016/j.nima.2008.11.056.

40 F. B. Araoz, M. Varini, A. Lundblad, S. Cabrera and G. Lindbergh, Effect of Partial Cycling of NCA/Graphite Cylindrical Cells in Different SOC Intervals, *J. Electrochem. Soc.*, 2020, **167**, 040529, DOI: 10.1149/1945-7111/ab78fd.

41 Y. Q. Liao, H. Y. Zhang, Y. F. Peng, Y. G. Hu, J. D. Liang, Z. L. Gong, Y. M. Wei and Y. Yang, Electrolyte Degradation During Aging Process of Lithium-Ion Batteries: Mechanisms, Characterization, and Quantitative Analysis, *Adv. Energy Mater.*, 2024, **14**, 2304295, DOI: 10.1002/aenm.202304295.

42 G. Nagasubramanian, Two-and three-electrode impedance studies on 18650 Li-ion cells, *J. Power Sources*, 2000, **87**, 226–229, DOI: 10.1016/S0378-7753(99)00469-3.

43 D. Juarez-Robles, C. F. Chen, Y. Barsukov and P. P. Mukherjee, Impedance Evolution Characteristics in Lithium-Ion Batteries, *J. Electrochem. Soc.*, 2017, **164**, A837–A847, DOI: 10.1149/2.1251704jes.

44 N. Togasaki, T. Yokoshima, Y. Oguma and T. Osaka, Prediction of overcharge-induced serious capacity fading in nickel cobalt aluminum oxide lithium-ion batteries using electrochemical impedance spectroscopy, *J. Power Sources*, 2020, **461**, 228168, DOI: 10.1016/j.jpowsour.2020.228168.

45 I. A. Bobrikov, N. Y. Samoylov, S. V. Sumnikov, O. Y. Ivanshina, R. N. Vasin, A. I. Beskrovnyi and A. M. Balagurov, *In situ* time-of-flight neutron diffraction study of the structure evolution of cathode, *J. Power Sources*, 2018, **372**, 74–81, DOI: 10.1016/j.jpowsour.2017.10.052.

46 S. P. Kühn, K. Edström, M. Winter and I. Cekic-Laskovic, Face to Face at the Cathode Electrolyte Interphase: From Interface Features to Interphase Formation and Dynamics, *Adv. Mater. Interfaces*, 2022, **9**, 2102078, DOI: 10.1002/admi.202102078.

47 W. M. Dose, W. Li, I. Temprano, C. A. O'Keefe, B. L. Mehdi, M. F. L. De Volder and C. P. Grey, Onset potential for Electrolyte Oxidation and Ni-Rich Cathode Degradation in Lithium-Ion Batteries, *ACS Energy Lett.*, 2022, **7**, 3524–3530, DOI: 10.1021/acsenergylett.2c01722.

48 H. Kawaura, M. Harada, Y. Kondo, H. Kondo, Y. Suganuma, N. Takahashi, J. Sugiyama, Y. Seno and N. L. Yamada, *Operando* Measurement of Solid Electrolyte Interphase Formation at Working Electrode of Li-Ion Battery by Time-Slicing Neutron Reflectometry, *ACS Appl. Mater. Interfaces*, 2016, **15**, 9540–9544, DOI: 10.1021/acsami.6b01170.

49 O. C. Harris, S. E. Lee, C. Lees and M. Tang, Review: mechanisms and consequences of chemical cross-talk in advanced Li-ion batteries, *J. Phys. Energy*, 2020, **2**, 032002, DOI: 10.1088/2515-7655/ab8b68.

50 R. Sahore, F. Dogan and I. D. Bloom, Identification of Electrolyte-Soluble Organic Cross-Talk Species in a Lithium-Ion Battery via a Two-Compartment Cell, *Chem. Mater.*, 2019, **31**, 2884–2891, DOI: 10.1021/acs.chemmater.9b00063.

51 S. Fang, D. Jackson, M. L. Dreibelbis, T. F. Kuech and R. J. Hamers, Anode-originated SEI migration contributes to formation of cathode- electrolyte interphase layer, *J. Power Sources*, 2018, **373**, 184–192, DOI: 10.1016/j.jpowsour.2017.09.050.

52 R. C. McNulty, E. Hampson, L. N. Culter, C. P. Grey, W. M. Dose and L. R. Johnson, Understanding the limits of Li-NMC811 half-cells, *J. Mater. Chem. A*, 2023, **11**, 18302–18312, DOI: 10.1039/d3ta00912b.